Environmental Science and Ecotechnology 20 (2024) 100356

Contents lists available at ScienceDirect

Environmental Science and Ecotechnology

journal homepage: www.journals.elsevier.com/environmental-science-and-ecotechnology/

Original Research

Water self-purification via electron donation effect of emerging contaminants arousing oxygen activation over ordered carbon-enhanced CoFe quantum dots

Yuhao Shi [1], Dongxuan Yang [1], Chun Hu, Lai Lyu*

Institute of Environ. Res. at Greater Bay Area, Key Laboratory for Water Quality and Conservation of the Pearl River Delta, Ministry of Education, Guangzhou University, Guangzhou, 510006, China

ARTICLE INFO

Article history:
Received 17 June 2023
Received in revised form
22 November 2023
Accepted 23 November 2023

Keywords:
Quantum dots
Emerging contaminants removal
Self-purification system
Dissolved oxygen

ABSTRACT

The release of emerging contaminants (ECs) into aquatic environments poses a significant risk to global water security. Advanced oxidation processes (AOPs), while effective in removing ECs, are often resource and energy-intensive. Here, we introduce a novel catalyst, CoFe quantum dots embedded in graphene nanowires (CoFeQds@GN-Nws), synthesized through anaerobic polymerization. It uniquely features electron-rich and electron-poor micro-regions on its surface, enabling a self-purification mechanism in wastewater. This is achieved by harnessing the internal energy of wastewater, particularly the bonding energy of pollutants and dissolved oxygen (DO). It demonstrates exceptional efficiency in removing ECs at ambient temperature and pressure without the need for external oxidants, achieving a removal rate of nearly 100.0%. The catalyst's structure-activity relationship reveals that CoFe quantum dots facilitate an unbalanced electron distribution, forming these micro-regions. This leads to a continuous electron-donation effect, where pollutants are effectively cleaved or oxidized. Concurrently, DO is activated into superoxide anions ($O_2^{\bullet-}$), synergistically aiding in pollutant removal. This approach reduces resource and energy demands typically associated with AOPs, marking a sustainable advancement in wastewater treatment technologies.

1. Introduction

Emerging contaminants (ECs), such as endocrine disruptors, persistent pharmaceuticals, pesticides, and synthetic dyes, have been widely found in natural water environments [1–3]. Even trace amounts of ECs in the water environment can trigger bio-concentration and produce ecotoxicological effects, posing a serious threat to public water safety [4–6]. Human exposure to ECs primarily occurs through ingesting food and beverages associated with contaminated soil, water, plants, animals, and microorganisms. Due to their hydrophobic properties, ECs tend to accumulate in biological tissues with high lipid content. In particular, species at the top of the food chain exhibit increasing bioaccumulation and biomagnification [7,8]. The specific harms to humans are manifested in disruptions to the endocrine and immune system, often involving the mimicry, suppression, or alteration of hormone function. These disruptions can lead to delayed brain development, premature puberty in children, reproductive issues, and an elevated risk of cancer and its associated complications [9,10]. However, removing ECs poses a formidable challenge, both in terms of relying on nature's self-purification abilities and the conventional wastewater treatment processes deployed in municipal wastewater treatment plants [11–13]. Despite the utilization of relatively uncomplicated and cost-effective technologies in contemporary wastewater treatment plants, the effective elimination of ECs remains an elusive goal. This is primarily attributed to the exceedingly low-level concentrations of ECs in water, the intricate composition of the actual wastewater, and the inherent resistance of ECs to biodegradation, which significantly hampers their removal through biological treatment methods [13–16]. In addition, physical and chemical methods, such as coagulation and sedimentation, struggle to yield satisfactory results (often less than 10% removal) due to the polarity and high water solubility of ECs

* Corresponding author.
E-mail address: lyulai@gzhu.edu.cn (L. Lyu).
[1] Authors contributed equally towards this study.

https://doi.org/10.1016/j.ese.2023.100356

[16–19].

Advanced oxidation processes (AOPs) are considered promising processes for the removal of ECs due to their capacity to initiate the degradation of these pollutants through the generation of various reactive oxygen species (ROS) during the reaction [20–24]. However, the high efficiency of AOPs comes at the expense of high energy and resource consumption. Commonly used AOPs, such as photocatalysis, Fenton/Fenton-like reactions, and peroxymonosufate (PMS) activation, require additional oxidants or external energy (light, electricity, ultrasound, etc.) during the process of degrading pollutants [25–29]. The exploration of AOPs that entail minimal or no additional oxidants or external energy remains underexplored. Therefore, there is an urgent need to develop new water treatment technologies to reduce energy and oxidant inputs while simultaneously achieving high-efficiency and low-energy consumption wastewater treatment processes.

In fact, wastewater contains abundant internal energy, such as the bond energy of organic pollutants and dissolved oxygen (DO). Reducing resource and energy consumption during wastewater treatment by fully utilizing the internal energy in the wastewater is a promising approach. However, ECs are extremely stable and difficult to degrade under natural conditions, thereby impeding the harnessing of the bonding energy of pollutants. Thus, it becomes imperative to reduce the bonding energy of ECs by activating ECs molecules preferentially through interfacial processes. In addition, despite the abundant presence of DO in water, its utilization under natural conditions remains a complex task. This is primarily due to the innate inertness of molecular oxygen in its ground state, necessitating the use of external inducers, such as light or electricity, to change the electrostatic potential distribution on the catalyst surface, thereby activating DO. It is a challenge to construct an unbalanced distribution of electrons on the catalyst surface by modulating the catalyst structure to utilize the bonding energy of ECs and activate DO in the absence of an inducer. According to molecular orbital theory, a molecular orbital is a linear combination of atomic orbitals in a molecule, which can form bonding molecular orbitals (e.g., σ and π orbitals) and antibonding molecular orbitals (e.g., σ* and π* orbitals). Similarly, in solid materials, the overlap of different kinds of atomic orbitals leads to strong interactions at the molecular orbital level, and based on this property, electrons can form a non-equilibrium and polarized distribution on the material surface. In particular, the cation-π interaction is one of the most important intermolecular binding forces between cations and electron-rich π orbitals [30]. The electron transfer forms of the orbital interaction of cation-π often involve π → cation (σ donation) and cation → π* (π antidonation) [30]. Interfacial confinement can fundamentally alter the energy of cation-π-mediated assemblies, which has been demonstrated [31]. Thus, polarity enhancement regulation of electrons and energy on the material surface by cation-π interactions is promising. Our previous work found that during the activation of H_2O_2 and PMS, the dual-reaction centers (DRCs) catalysts formed by combining molecular orbital theory to construct electron-poor/rich micro-regions on the catalyst surface can trigger the electron-donation effect of pollutants (pollutants are thus oxidized or cleaved) and DO can also be activated to generate ROS ($O_2^{\bullet-}$, •OH, and $^1O_2$) to attack the pollutants [32–39]. This suggests that constructing a cation-π structure is a feasible strategy for inducing an unbalanced distribution of electrons on the catalyst surface to activate dissolved oxygen. However, in our prior research, initiating these effects still necessitated a minimal infusion of external energy for activation.

In this work, CoFe quantum dots DRCs catalyst with cation-π structure (CoFeQds@GN-Nws) was successfully developed by anaerobic polymerization, which can directly utilize the energy of DO and the bond energy of pollutants in water to realize the self-purification process of wastewater without additional oxidants or external energy. CoFeQds@GN-Nws exhibited excellent removal performance for various types of ECs and showed excellent catalytic activity in different pH ranges as well as in the presence of different salts, even showing extremely strong purification performance for actual industrial dyeing wastewater. CoFeQds@GN-Nws self-purification system breaks through the limitation of AOPs requiring external oxidant or external energy. Under natural conditions, without additional oxidants or external energy, CoFeQds@GN-Nws can trigger the continuous electron-donation effect of pollutants. This effect results in the cleavage and oxidation of contaminants while simultaneously activating DO, leading to the generation of $O_2^{\bullet-}$ that synergistically removes pollutants. The resource and energy consumption of the wastewater self-purification process occurring under the CoFeQds@GN-Nws system is greatly reduced compared to conventional water treatment technologies, which is consistent with achieving carbon neutrality and emissivity peak [40].

2. Materials and methods

2.1. Preparation of catalysts

CoFeQds@GN-Nws was developed by an anaerobic polymerization process (Scheme 1). Firstly, 6.5 g 2-methylimidazole and 3 g $Zn(NO_3)_2{\cdot}6H_2O$ were dissolved in 120 mL methanol with stirring. Then, to construct the inhomogeneity of electrons on the catalyst surface, two metal sources with different electronegativity (0.88 g $Fe(acac)_3$ and 0.58 g $Co(NO_3)_2{\cdot}6H_2O$) were added to the above solution and stirred at room temperature for 24 h. The obtained products were centrifuged and washed with ethanol, then placed in a vacuum drying oven at 60 °C until completely dried. Then, to form a cationic π-structure, the dried product was put into a tube furnace, pyrolysis at 900 °C for 1 h in a flowing nitrogen atmosphere, after high-temperature polymerization and annealing to obtain CoFeQds@GN-Nws. The comparison samples, Fe@GN, Co@GN, and GN, were prepared similarly. The detailed steps are provided in the Supplementary Material.

2.2. Procedures and analysis

Based on this innovative catalyst (CoFeQds@GN-Nws), a self-purification system for wastewater was established. The wastewater treatment performance of the CoFeQds@GN-Nws was investigated under natural conditions by treating actual dyeing wastewater and removing several ECs, such as endocrine disrupting chemical bisphenol A (BPA), persistent drug diphenhydramine (DP), herbicide atrazine (ATZ), and synthetic dye rhodamine B

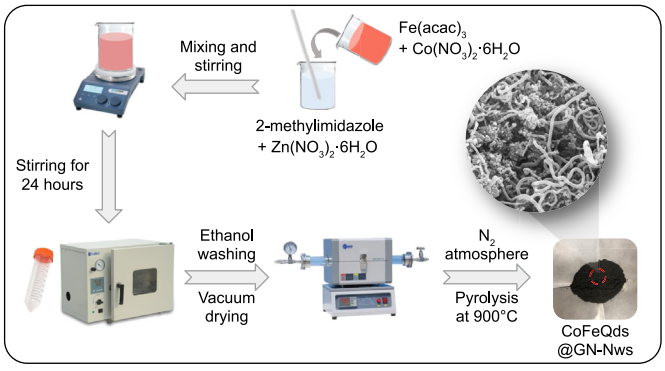

Scheme 1. A schematic illustration of the synthesis process of CoFeQds@GN-Nws.

(RhB). The structures of these pollutants are shown in Fig. S1. The optimal dosages of catalyst powder (0.6 g L^{-1}, Fig. S2) were used in all experiments unless otherwise specified. In a typical experiment, 50 mL of the pollutant aqueous solution (concentration: 10 mg L^{-1}) and 0.03 g of the catalyst powder were placed in a beaker. The whole experiment was carried out under ambient air conditions and magnetic stirring. At given time intervals, 1 mL of the reaction solution was collected and filtered through a Millipore filter (pore size: 0.45 μm, Jinteng, China) for analysis. The durability and stability of CoFeQds@GN-Nws were tested by an innovative fixed-bed reactor. All information for the sample preparation and measurement is shown in the Supplementary Material.

3. Results and discussion

3.1. Water self-purification system construction and performance

A self-purification system without any external energy was constructed to evaluate the wastewater treatment performance of the innovative CoFeQds@GN-Nws. Typically, in normal temperature, normal pressure, and air conditions, only a small amount of CoFeQds@GN-Nws (0.6 g L^{-1}) was added to the suspension of pollutants. Remarkably, within this system, the removal of ECs, such as ATZ, BPA, RhB, and DP, occurred expeditiously. In the absence of additional oxidants or external energy, the removal rates of ATZ, BPA, and RhB exceed 78.0% in only 5 min, complete decolorization of RhB is achieved within only 30 min, and complete removal of BPA is achieved within only 60 min, the removal rate of ATZ reached 96.1% and 69.3% for DP in 120 min (Fig. 1a), which is the first reported CoFe quantum dots catalyst self-purification system with excellent ECs removal performance. In contrast, the comparison samples are much less effective in removing pollutants than CoFeQds@GN-Nws, especially Co@GN, which was only 26.2% removal of BPA after 120 min (Fig. S3). This indicates that the CoFeQds@GN-Nws system exhibits excellent removal effects on various pollutants without additional oxidants or external energy. The underlying mechanism of wastewater purification by the CoFeQds@GN-Nws self-purification system was revealed by reaction under air and N_2 conditions. In the N_2 condition, the DO concentration diminished, resulting in a corresponding inhibition of BPA removal (Fig. 1b). The rate constant in the air condition is 186.8% higher than in the N_2 condition, indicating that DO is involved in the removal process and is a key factor in the reaction.

To evaluate the adaptability of CoFeQds@GN-Nws to complex water environmental media, experiments on the effect of initial pH and different salts (anions) were carried out. As shown in Fig. 1c, the catalytic activity of the catalyst was not inhibited in a wide pH range (pH = 3–11), and BPA could still be completely removed in the CoFeQds@GN-Nws system within 120 min even in the pH range of extremely acidic and alkaline. Moreover, the self-purification process of the CoFeQds@GN-Nws system is not significantly affected in the presence of different salts (Fig. 1d). The removal rate of BPA in the presence of SO_4^{2-}, PO_4^{3-}, and NO_3^- still reached 100.0%, and even in the presence of the most significantly inhibited CO_3^{2-} the removal rate of BPA is as high as ~70.0% within 120 min. These results indicate that the wastewater self-purification process is adaptable and can achieve efficient pollutant removal in complex water environments. The performance of the actual wastewater treatment was further investigated by actual industrial dyeing wastewater (from a dyeing and printing industrial park in Puning, China). Analysis of changes in the water environment during the self-purification process by 3D fluorescence technology (Fig. 1e and f), the intensity of fluorescence peaks corresponding to substances, such as fulvic acid, humic acid, and microbial metabolites in water,

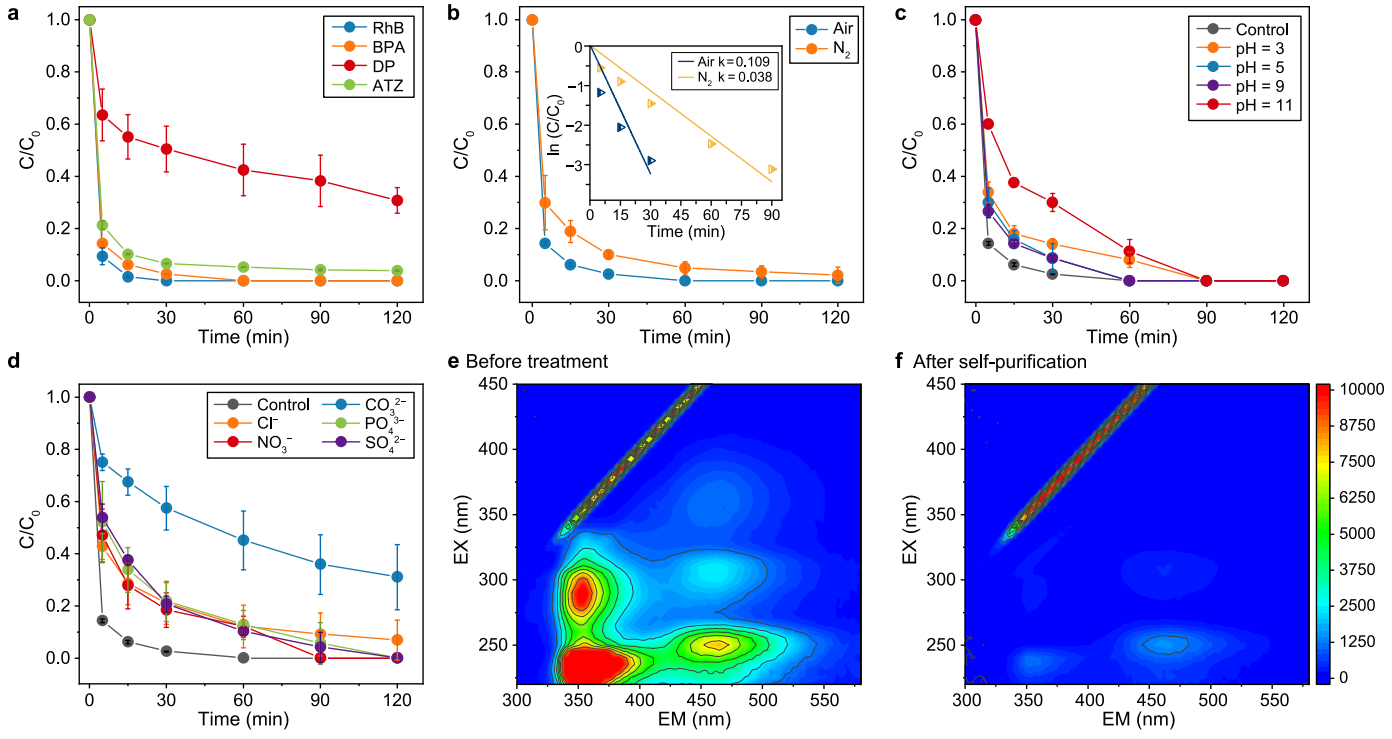

Fig. 1. **a**, Removal of different pollutants in the CoFeQds@GN-Nws suspension. **b**, BPA removal in air and N_2 atmospheres (the inserted figure shows pseudo-first-order kinetic rate plots of pollutant removal in the CoFeQds@GN-Nws system). **c**, Effect of initial pH on BPA removal using CoFeQds@GN-Nws. **d**, BPA removal using CoFeQds@GN-Nws in the presence of different anions. **e**, 3D-EEM fluorescence spectra of actual dyeing wastewater. **f**, 3D-EEM fluorescence spectra of actual dyeing wastewater after self-purification reaction. Reaction conditions: initial pH 6.5 (nature pH), pollutants 10 ppm, catalyst 0.6 g L^{-1}, initial temperature 30 °C.

was significantly weakened after 120 min, indicating that the self-purification process showed outstanding treatment effect on the actual wastewater treatment. The ability of the CoFeQds@GN-Nws system to remove ECs without additional oxidants or external energy in a natural water environment (Pearl River water in Guangzhou, China) was investigated. A comparison of the 3D-EEM (Excitation-Emission Matrix Fluorescence) fluorescence spectra before and after the self-purification process (Fig. 2a and b) showed that the fluorescence peak caused by BPA disappeared completely after 120 min, indicating that the CoFeQds@GN-Nws system showed excellent ability to remove ECs in a natural water environment. Surprisingly, the fluorescence peaks in uncontaminated Pearl River water (Fig. 2c) did not disappear after the self-purification process, which indicates that the CoFeQds@GN-Nws system preferentially removed ECs from the water in the natural water environment without causing damage to the natural water environment, showing great prospects for practical water treatment applications.

The stability and durability of the catalyst were investigated by constructing a fixed-bed reactor (with CoFeQds@GN-Nws as the core filler) (Fig. 2d) to simulate the operation of tertiary treatment of wastewater containing the endocrine-disrupting chemical. As shown in Fig. 2e, the catalyst activity of the self-purification system was maintained at a high level after 720 min of continuous operation (~12 times cycle), and the removal rate of BPA was maintained above 90.0%, indicating that CoFeQds@GN-Nws is a stable and efficient catalyst.

3.2. Structure characterization and structure-activity relationship

The scanning electron microscopy (SEM) images (Fig. 3a and b) show that the catalyst forms an elongated carbon nanowire structure, and transmission electron microscopy (TEM) images of the catalyst (Fig. 3c) further reveal that these carbon nanowires are grown in situ on the catalyst surface. Meanwhile, many obvious black CoFe nanoparticles are observed in Fig. 3d. The TEM elemental mappings (Fig. 3e) of CoFeQds@GN-Nws show that C, O, N, and Zn are uniformly dispersed in the particle bulk, the Co and Fe are almost dispersed at the same position, which explicitly confirms the formation of CoFe nanoparticles [41]. High-resolution transmission electron microscopy (HRTEM) image of CoFeQds@GN-Nws (Fig. 3f) shows clear lattice stripes. The measured lattice stripe spacing of 0.20 and 0.33 nm can be attributed to the (002) crystal plane of graphitic carbon and the (110) crystal plane of CoFe nanoparticles. Meanwhile, it can be clearly seen in the HRTEM image that the diameter of the CoFe nanoparticle is ~5.00 nm. This indicates that CoFeQds@GN-Nws forms a CoFe quantum dot structure. Fig. 4g and h shows the powder X-ray diffraction (XRD) patterns of CoFeQds@GN-Nws and the comparison samples. The introduction of Co and Fe resulted in a distinctly different structure of the CoFeQds@GN-Nws. Three diffraction peaks of CoFeQds@GN-Nws at 44.7°, 65.0°, and 82.6° are attributed to (110), (200) and (211) diffraction of CoFe nanoparticles (PDF-#49−1568), and the diffraction peaks near 26.0° are attributed to the graphite C (PDF-#41−1487), indicating the formation of CoFe alloy structure and revealing the carbonaceous feature of the CoFeQds@GN-Nws. In addition, the XRD pattern of the CoFeQds@GN-Nws after activity evaluation experiments did not have obvious change compared to the fresh sample (Fig. 4g), which indicated that the catalyst formed a stable crystal phase structure, and thus CoFeQds@GN-Nws exhibit excellent stability and durability in the stability evaluation experiment.

The X-ray photoelectron spectroscopy (XPS) survey spectrum in Fig. S4 shows that CoFeQds@GN-Nws contained Co, Fe, Zn, C, N, and O elements. The peak at 779.2 eV in the Co 2p XPS spectrum of CoFeQds@GN-Nws (Fig. 4a) corresponds to the $2p_{3/2}$ and $2p_{1/2}$ of zero valence cobalt [42]. The peaks at 707.0 eV in the Fe 2p XPS spectrum of CoFeQds@GN-Nws (Fig. 4b) can be deconvoluted into Fe^0 $2p_{3/2}$ [42]. The new appearance of zero valence iron in CoFeQds@GN-Nws compared with Fe@GN indicated that the addition of Co led to an increase in the reduced state of Fe and electrons accumulation, thus changing the potential difference of

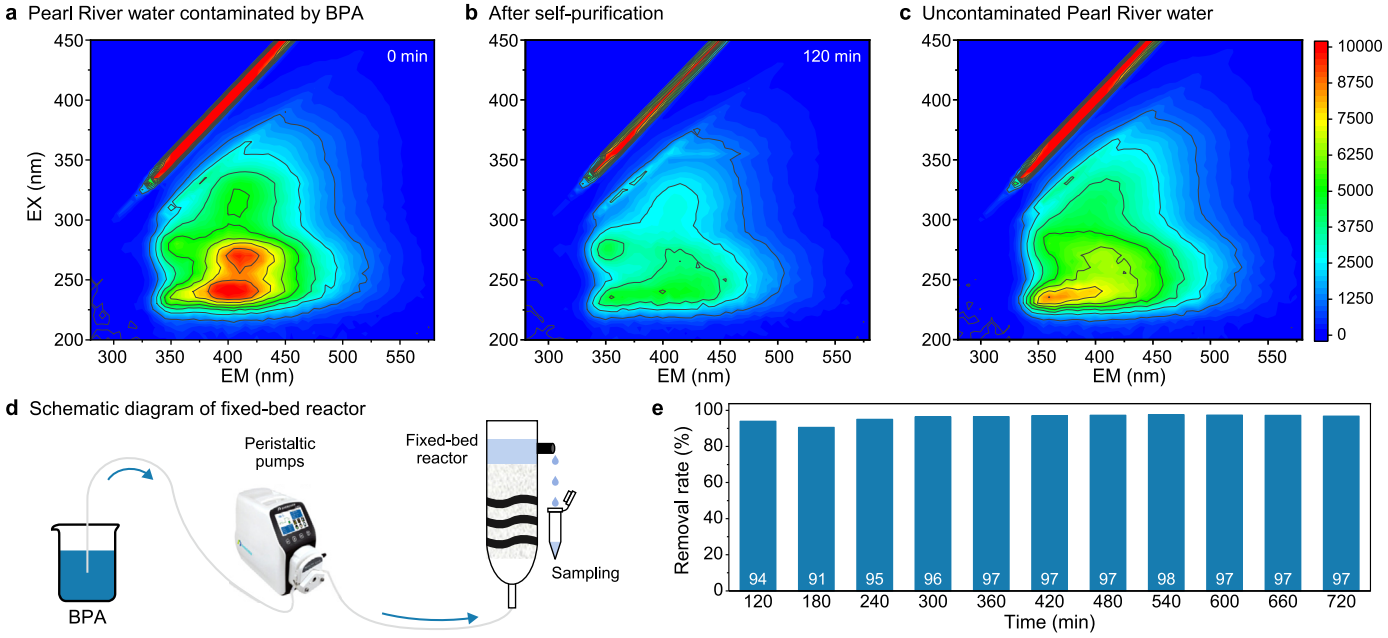

Fig. 2. **a**, 3D-EEM fluorescence spectra of Pearl River water contaminated by BPA. **b**, 3D-EEM fluorescence spectra of Pearl River water contaminated by BPA after self-purification. **c**, 3D-EEM fluorescence spectra of uncontaminated Pearl River water. **d**, Schematic diagram of fixed-bed reactor. **e**, Stability and durability performance of BPA removal in a fixed bed reactor using CoFeQds@GN-Nws system. Reaction conditions: initial pH 6.5 (nature pH), pollutants 10 ppm, catalyst 0.6 g L^{-1}, initial temperature 30 °C, hydraulic retention time 60 min.

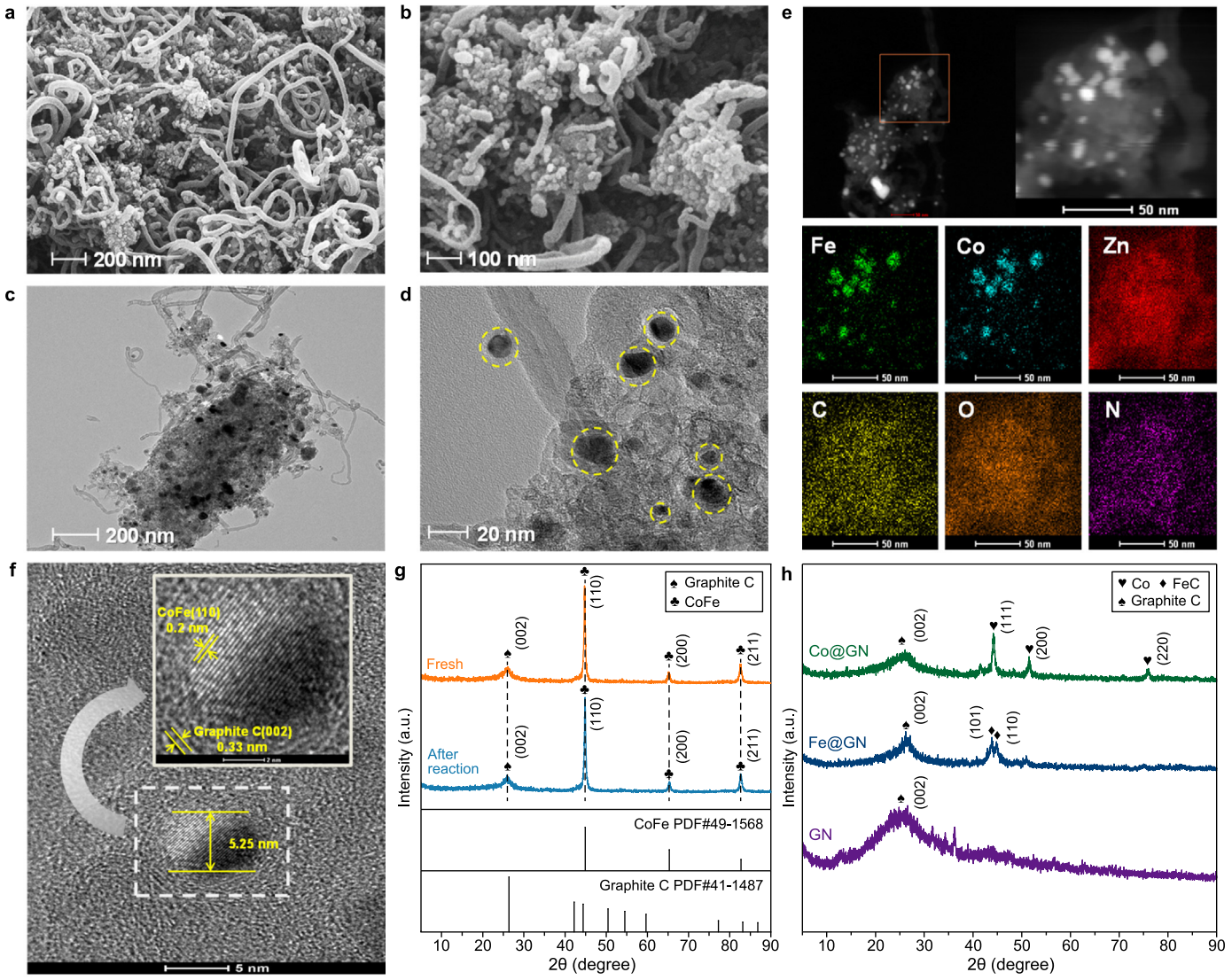

Fig. 3. **a**–**b**, SEM images of CoFeQds@GN-Nws with a scale bar of 200 nm (**a**) and 100 nm (**b**). **c**–**d**, TEM images of CoFeQds@GN-Nws with a scale bar of 200 nm (**c**) and 20 nm (**d**). **e**, TEM elemental mapping of CoFeQds@GN-Nws. **f**, HRTEM images of CoFeQds@GN-Nws. **g**, XRD patterns of CoFeQds@GN-Nws (fresh and after reaction). **h**, XRD patterns of Co@GN, Fe@GN, and GN.

the original site, making a larger potential difference at the CoFe site, and making the reduction of DO possible. The appearance of zero valence Fe and Co further confirms the formation of CoFe alloy particles in CoFeQds@GN-Nws, the strong interactions between CoFe and the surrounding C, N, and O atoms make the appearance of Co and Fe in an oxidation state [43]. In the Zn 2p XPS spectrum (Fig. 4c), two peaks appeared at 1022.0 and 1045.1 eV, corresponding to Zn^{2+} $2p_{3/2}$ and Zn^{2+} $2p_{1/2}$, respectively. The peak intensity of CoFeQds@GN-Nws was significantly lower than the comparison samples, indicating that adding Fe and Co atoms replaced part of the originally present Zn atoms [12]. The N 1s XPS spectrum of CoFeQds@GN-Nws (Fig. 4d) fitted into four peaks at 399.3, 398.6, 401.1, 402.6 eV, which are ascribed to pyridinic N, pyrrolic N, graphitic N and oxidized N, respectively [44]. Graphite N and pyridinic N can effectively enhance the activity of oxygen reduction reactions. In addition, CoFeQds@GN-Nws has the highest relative content of graphite N and pyridinic N compared with the comparison samples, which indicated that CoFeQds@GN-Nws has a better catalytic ability of oxygen reduction reaction [45,46]. In the O 1s XPS spectrum of CoFeQds@GN-Nws (Fig. 4e), the peaks at 530.9 and 533.3 eV corresponded respectively to the lattice oxygen and surface oxygen, and the peak at 532.2 eV between the lattice oxygen and surface oxygen corresponded to C–O-M bonds (M stands for metal). The C 1s XPS spectrum of CoFeQds@GN-Nws (Fig. 4f) can be fitted into three peaks at 284.7 (C–C/C=C bonds), 285.6 (C–O/C–N bonds) and 289.6 eV (C=O bonds). The presence of C–C/C=C bonds indicated the formation of aromatic C(π) structures. The C–O peaks of CoFeQds@GN-Nws have higher binding energy than GN and Fe@GN, indicating the formation of a C–O–M bonding linkage, which corresponds to the XPS spectrum of O 1s, and further verified the formation of cation-π structure [47]. In addition, the C–O/C–N bonds and C=O bonds contents of CoFeQds@GN-Nws are lower compared with the comparison samples, indicating that CoFeQds@GN-Nws has a higher degree of graphitization and stronger electron transport capacity, which is beneficial to the activity of the DO reduction reaction and the electron-donation effect of ECs [48].

In the Raman spectra, it can be clearly seen that two graphene-like carbon characteristic peaks appear around 1342 and 1580 cm^{-1} (Fig. 5a), which represent the D-band corresponding the defects/

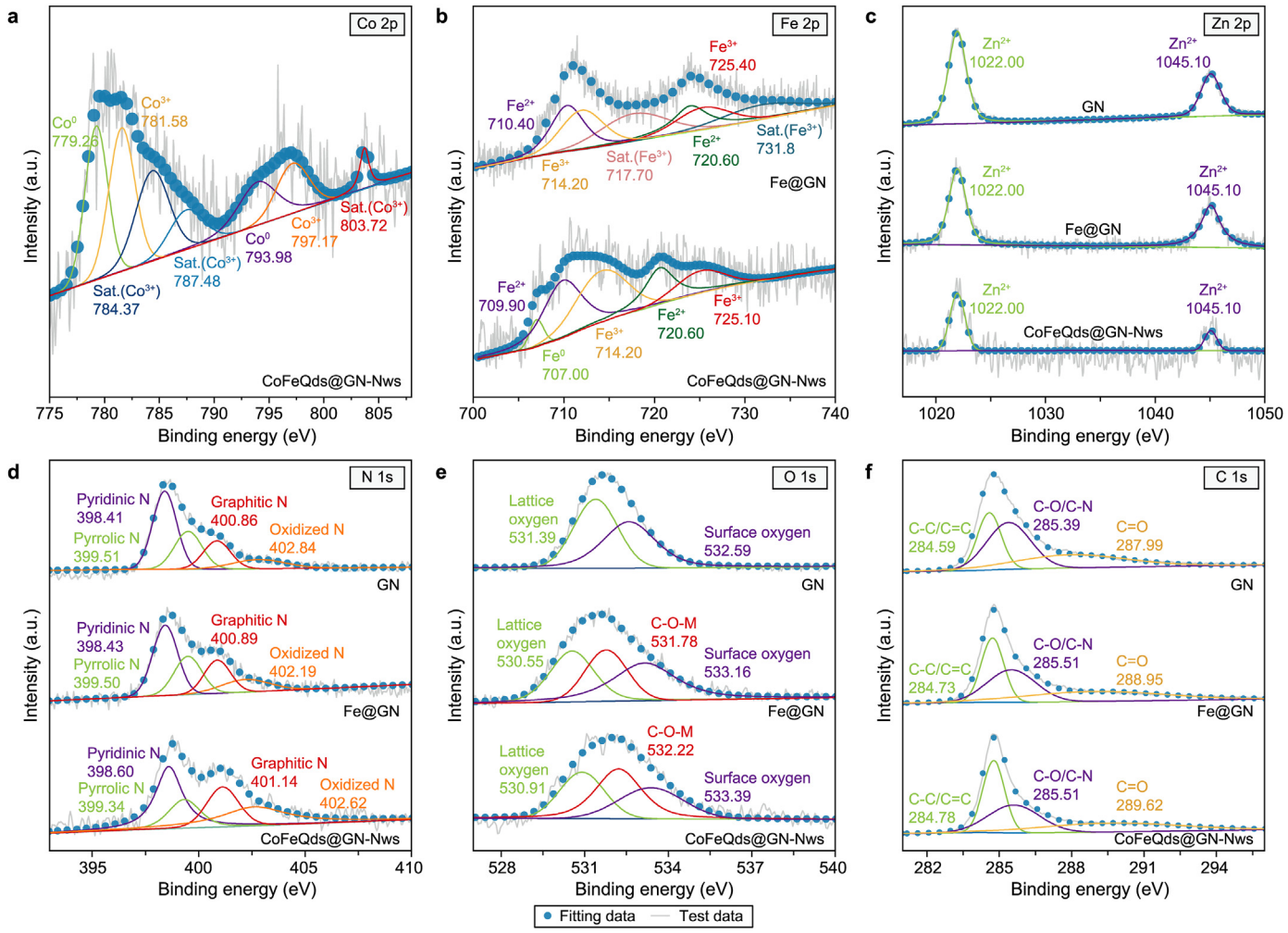

Fig. 4. **a**, Co 2p XPS spectra of CoFeQds@GN-Nws. **b**, Fe 2p XPS spectra of CoFeQds@GN-Nws and Fe@GN. **c**–**f**, Zn 2p (**c**), N 1s (**d**), O 1s (**e**), and C 1s (**f**) XPS spectra of CoFeQds@GN-Nws, Fe@GN, and GN.

distortion of the crystal lattice for sp^3-hybridized C atoms and G-band attributed to the active E_{2g} vibration of the sp^2-hybridized C atoms, respectively, thus confirming the formation of a typical graphene-like carbon structure of the catalyst [32,49]. By comparing the I_D/I_G ratio of all samples, it was found that the introduction of Fe affects both the defects and the degree of graphitization, making some of the original defect sites occupied and making a higher degree of graphitization to form a better graphene-like structure (aromatic C(π) structures). The introduction of Co has led to a change in the defect sites based on retaining the original well-formed graphene-like carbon structure. The I_D/I_G ratio of CoFeQds@GN-Nws (1.04) is lower than the other comparison samples, indicating that CoFeQds@GN-Nws has a higher degree of graphitization and better electrical conductivity, which was caused by the formation of more carbon nanowires in the catalyst due to the catalytic effect of the transition metal [50]. In addition, the D and G bands were shifted after the addition of Fe and Co, indicating that both Fe and Co entered inside the catalyst and formed a bond between the metal and graphene-like carbon, which led to the rearrangement of the catalyst electrons and the unbalanced electron distribution, and this is the key factor leading to the excellent performance of the catalyst.

The Fourier transform infrared spectroscopy (FTIR) of CoFeQds@GN-Nws is shown in Fig. S5. The absorption bands in the range of 1147–1544 cm^{-1} are attributed to the C–N stretching vibrations. These peaks are significantly weakened and blue-shifted to higher wavenumbers in CoFeQds@GN-Nws compared to the comparison samples due to the introduction of metal atoms leading to a reduction in C–N content or C–N bonding with metals [51]. The wavenumber of the hydroxyl vibration peak in CoFeQds@GN-Nws was shifted to 3423 cm^{-1}, and a new hydroxyl vibration peak appeared (3733 cm^{-1}) compared to the comparison samples due to the strong interaction between the GN substrate and Co, Fe species which confirmed the successful introduction of metal atoms [52]. In addition, this phenomenon suggests that the CoFe sites formed in the catalyst may be more likely to contact ECs containing O and Cl groups, and promote the electron donation effect of ECs containing these groups on the catalyst surface. Thus, ECs can be removed by cleavage on the catalyst surface. This is consistent with the experimental results of the activity evaluation of the CoFeQds@GN-Nws self-purification system. The removal rate of DP (without s surface groups) is slower, whereas BPA, RhB, and ATZ (containing O or Cl groups) are removed more rapidly. The H_2-temperature programmed reduction (H_2-TPR) technique further confirmed the presence of various metals in different valence states in CoFeQds@GN-Nws. The presence of reduction peaks for each valence state of Co, Fe, and Zn in the H_2-TPR results (Fig. 5b) proved the presence of various valence states of metals in the catalyst. The

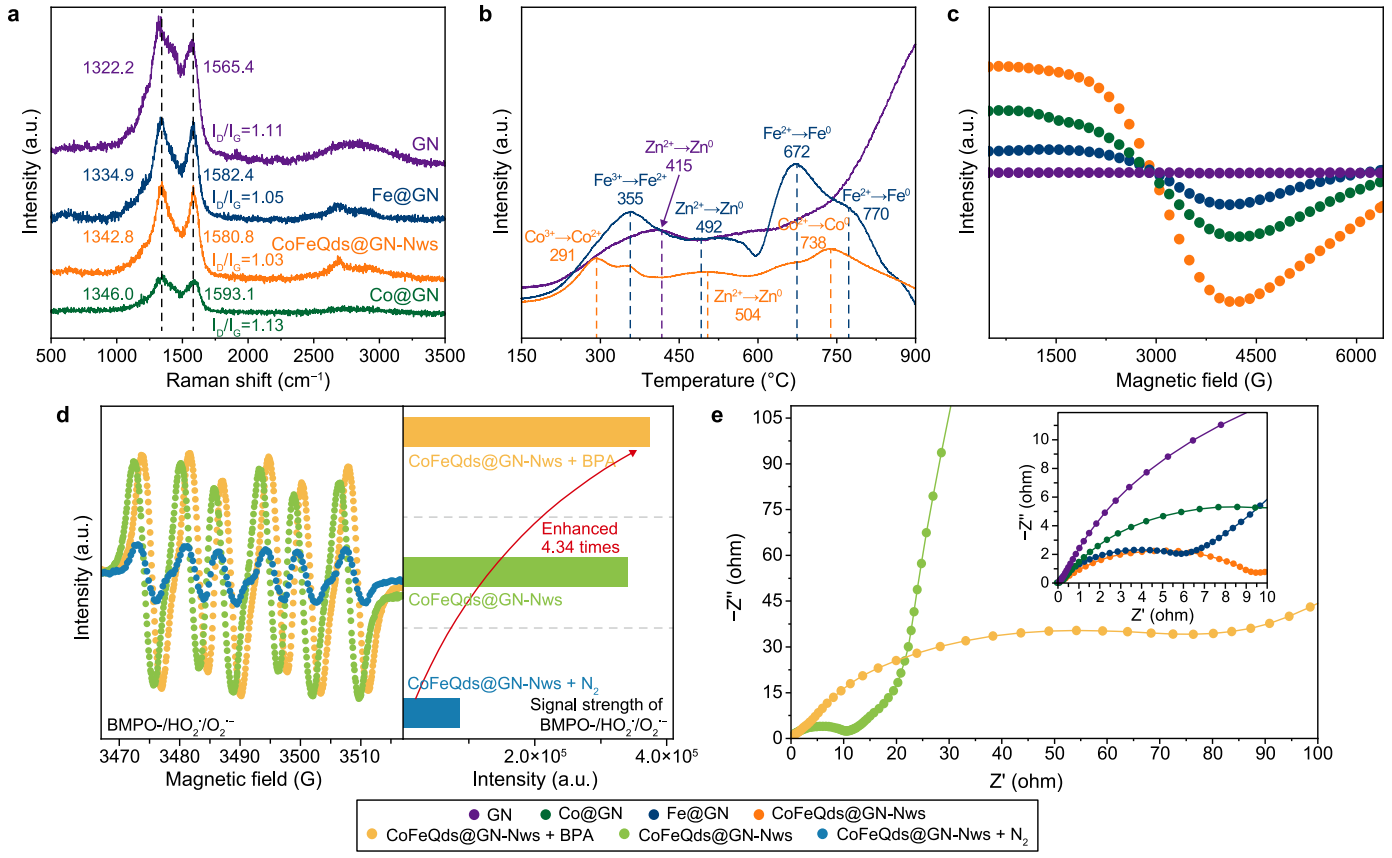

Fig. 5. **a**, Raman spectra of CoFeQds@GN-Nws, Fe@GN, Co@GN, and GN. **b**, H_2-TPR curves of CoFeQds@GN-Nws, Fe@GN, and GN. **c**, EPR spectra of the CoFeQds@GN-Nws, Fe@GN, Co@GN, and GN solid samples. **d**, BMPO spin-trapping EPR spectra in methanol for $^{\bullet}OH_2/O_2^{\bullet-}$. **e**, EIS spectra of the CoFeQds@GN-Nws electrode in different systems (the inserted figure shows EIS spectra of the CoFeQds@GN-Nws, Co@GN, Fe@GN, and GN electrodes). Reaction conditions: initial pH 6.5 (nature pH), pollutants 10 ppm, catalyst 0.6 g L^{-1}, Na_2SO_4 = 0.1 M, initial temperature 30 °C.

reduction temperature of Co and Fe in the higher valence state is lower compared to the corresponding oxides of Co and Fe, indicating that the Co and Fe in the catalyst form a more stable structure than the oxides, further confirming the formation of the C—O—M bond linkage [12,53–56]. In addition, the reduction peaks of $Zn^{2+}\rightarrow Zn^0$ shifted to the high-temperature region after the introduction of Fe and Co, indicating that Zn was protected, more difficult to reduce, and became the substrate for the catalyst to make the catalyst structure more stable, while Co and Fe were the main active sites of the catalyst.

Electron paramagnetic resonance (EPR) spectroscopy was used to detect and analyze the signal of unpaired single electrons on the catalyst surface. As shown in Fig. 5c, no signal of unpaired electrons was detected on GN, and a high intensity of unpaired electrons signal was detected on CoFeQds@GN-Nws, surpassing those observed in other comparative samples. Building upon our previous work, this result indicated that the lattice doping of Fe and Co completely changes the electron distribution on the catalyst, resulting in the formation of electron-rich Fe and Co micro-regions and electron-poor C(π) micro-regions in CoFeQds@GN-Nws [57–59]. The higher intensity of the unpaired electrons makes it easier for CoFeQds@GN-Nws to capture electrons from the pollutants during the reaction and facilitates the activation of DO.

3.3. Water self-purification mechanism of the CoFeQds@GN-Nws system

Following the previous analysis, it is known that DO and ECs are two important factors in the self-purification reaction process, which are the key to driving the reaction. In the context of the CoFeQds@GN-Nws self-purification system, we delve deeper into the interfacial reaction mechanism. The single-electron signal of CoFeQds@GN-Nws after the reaction was detected by EPR. As shown in Fig. S6, the single electron signal of the catalyst after the reaction was stronger than the fresh catalyst, indicating that the catalyst, DO, and pollutants undergo an evident electron transfer process during the reaction. The pollutants act as electron donors in the reaction to provide electrons to the catalyst, and the catalyst conveys electrons to DO, reducing it to $HO_2^{\bullet}/O_2^{\bullet-}$ and participating in the removal of pollutants. Furthermore, the single electron signal of the catalyst was increased largely after the reaction with 100 ppm of BPA, indicating that more electrons from pollutants not consumed by DO accumulate on the catalyst surface, further confirming the electron cycling process between the catalyst, DO, and pollutants.

The detection of ROS generated during the removal of pollutants by CoFeQds@GN-Nws, with BMPO (5-*tert*-Butoxycarbonyl-5-methyl-1-pyrroline-N-oxide) and TEMP (2,2,6,6-tetramethyl-4-piperidinol) as trapping agents. No significant TEMP-$^1O_2$ signal was detected in the aqueous medium (Fig. S7a). A very weak BMPO-$^{\bullet}$OH signal was detected in the aqueous medium, which came from the $^{\bullet}$OH generated by the cleavage of BPA on the surface of CoFeQds@GN-Nws (Fig. S7b). In contrast, a strong BMPO-$HO_2^{\bullet}/O_2^{\bullet-}$ signal was detected in the CoFeQds@GN-Nws system (in methanol medium) (Fig. 5d), indicating that the catalyst can activate DO to $HO_2^{\bullet}/O_2^{\bullet-}$ under natural conditions without additional

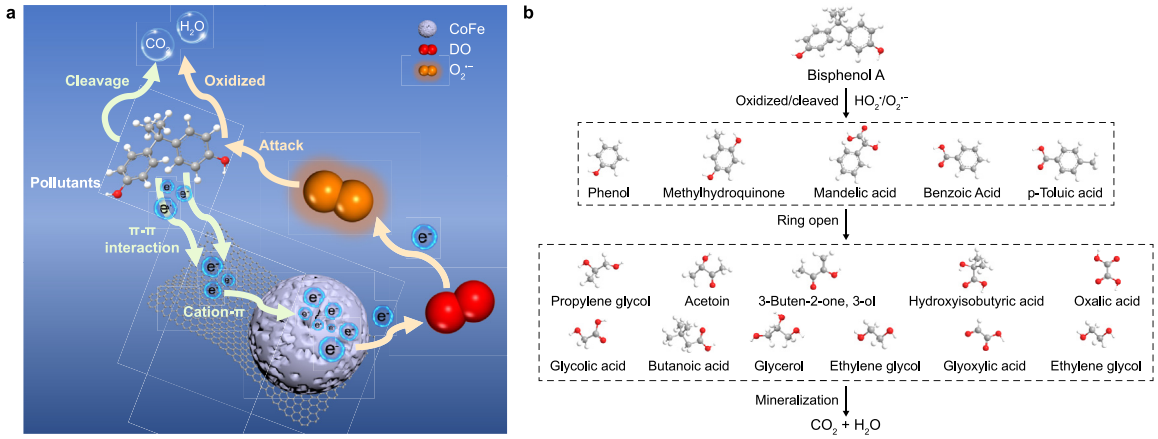

Fig. 6. **a**, A schematic diagram showing the interfacial reaction mechanism in the CoFeQds@GN-Nws/DO/pollutants self-purification system. **b**, Possible removal pathway of BPA in the CoFeQds@GN-Nws system.

oxidants or external energy. After adding BPA, the signal of the BMPO-$HO_2^{\bullet}/O_2^{\bullet-}$ became more significant instead of weakening (4.34 times higher than under N_2 conditions), indicating that electron transfer between BPA, DO, and catalyst occurred in the solid-water interface. During this process, BPA lost electrons (electron-donation effect) and passed to DO through the catalyst to produce more $HO_2^{\bullet}/O_2^{\bullet-}$. Under N_2 conditions, the signal intensity of BMPO-$HO_2^{\bullet}/O_2^{\bullet-}$ was much weaker than that detected in the air condition, indicating that DO is the main source of $HO_2^{\bullet}/O_2^{\bullet-}$ production during the reaction. Therefore, the removal of pollutants is inhibited in the N_2 condition due to the reduction of DO that can receive electrons from pollutants.

Fig. 5e (inserted) shows the electrochemical impedance spectra (EIS) of the CoFeQds@GN-Nws and comparison samples under the same conditions. Notably, CoFeQds@GN-Nws has the lowest impedance and the fastest electron transfer rate, indicating that CoFeQds@GN-Nws has excellent electron transfer capability. It is noteworthy that in Fig. 5e, the impedance of CoFeQds@GN-Nws is smaller in the solution without pollutant interference when Z′ is below 20, but the impedance of CoFeQds@GN-Nws is smaller in the presence of BPA after Z′ exceeds 20. Overall, in the presence of pollutants, CoFeQds@GN-Nws showed lower impedance and faster electron transfer rate, improving the removal efficiency of the pollutant self-purification system.

Combining the above analysis, $HO_2^{\bullet}/O_2^{\bullet-}$ is not a major pathway for degrading pollutants due to its low redox potential and weak removal ability [60]. Therefore, it is inferred that pollutants are primarily subjected to oxidation/cleavage by donating electrons to the catalyst through π-π interactions (electron-donation effect). Simultaneously, they are attacked by $HO_2^{\bullet}/O_2^{\bullet-}$ generated by the reduction of DO. This dual action expedites the removal of pollutants (Fig. 6a). With the synergistic effect of these two removal pathways, the rapid self-purification process of wastewater can be achieved at ambient temperature and pressure without additional oxidants or external energy.

To further clarify the self-purification mechanism, we assessed the catalyst's solid surface and liquid samples after a 30-min reaction with BPA as the target pollutant (Fig. S8). The possible removal pathways of BPA were inferred from the intermediates appearing in the gas chromatography-mass spectroscopy (GC-MS) results (Fig. 6b). The BPA initially underwent decomposition into phenol, benzoic acid, and mandelic acid through the synergistic effect of ROS attack and surface cleavage. Subsequently, it underwent ring-opened cleavage, giving rise to non-toxic small-molecule products, such as glycerol, acetoin, and ethylene glycol, and finally mineralized into CO_2 and H_2O. Pollutant removal pathway analysis further verified that CoFeQds@GN-Nws relies on the self-purification mechanism of internal energy in the water rather than only simple adsorption of pollutants.

4. Conclusion

In summary, we developed a novel DRCs catalyst (CoFeQds@GN-Nws) and presented the development of a self-purification system for wastewater treatment by adjusting the electron distribution on the catalyst surface. This system exhibited excellent removal performance for various types of ECs under natural conditions without requiring additional oxidant or external energy. The removal rate of most ECs reached over 95.0% within 120 min. Furthermore, the catalyst exhibits remarkable catalytic activity even in complex water environments, encompassing a wide pH range and the presence of various salts. Even after simulating 720 min of tertiary wastewater treatment, the removal rate for ECs remains above 90.0%, and it can purify actual dyeing wastewater within a mere 120 min. The formation of cation-π structure and electron-poor/rich micro-regions on the catalyst surface are the keys to the excellent performance of the catalyst, allowing CoFeQds@GN-Nws to trigger a continuous electron-donation effect of pollutants under natural conditions, activating DO into $O_2^{\bullet-}$ for synergistic removal of pollutants. The CoFeQds@GN-Nws self-purification system achieves high efficiency and low consumption, tapping into the internal energy in wastewater. This approach significantly reduces the resource and energy consumption of traditional water treatment processes, making quantum dot catalysts a promising solution for eliminating ECs from the actual water environment. Overall, this work provides insights into the creation of low-consumption DRCs water treatment systems and the efficient utilization of internal energy in water during wastewater treatment. Catalyst synthesis with lower resource and energy consumption needs to be explored in future research, as this holds significant promise for achieving carbon neutrality and emissivity peak goals.

CRediT authorship contribution statement

Yuhao Shi: Writing - Original Draft, Investigation, Data Curation, Visualization. **Dongxuan Yang:** Investigation, Data Curation, Visualization. **Chun Hu:** Project Administration, Funding Acquisition, Supervision. **Lai Lyu:** Conceptualization, Writing - Review & Editing, Supervision, Project Administration, Funding Acquisition.

Declaration of competing interest

The authors declare that they have no known competing financial interests or personal relationships that could have appeared to influence the work reported in this paper.

Acknowledgements

This work was financially supported by the National Natural Science Foundation of China (52350005, 52122009, 52070046, and 51838005), the Introduced Innovative Research and Development Team Project under the "Pearl River Talent Recruitment Program" of Guangdong Province (2019ZT08L387), and Basic and Applied Basic Research Project of Guangzhou (202201020163).

Appendix A. Supplementary data

Supplementary data to this article can be found online at https://doi.org/10.1016/j.ese.2023.100356.

References

[1] N. Morin-Crini, E. Lichtfouse, G. Liu, V. Balaram, A.R.L. Ribeiro, Z. Lu, F. Stock, E. Carmona, M.R. Teixeira, L.A. Picos-Corrales, J.C. Moreno-Piraján, L. Giraldo, C. Li, A. Pandey, D. Hocquet, G. Torri, G. Crini, Worldwide cases of water pollution by emerging contaminants: a review, Environ. Chem. Lett. 20 (4) (2022) 2311–2338.
[2] A. Pal, Y. He, M. Jekel, M. Reinhard, K.Y. Gin, Emerging contaminants of public health significance as water quality indicator compounds in the urban water cycle, Environ. Int. 71 (2014) 46–62.
[3] L. Zhu, C. Jiang, S. Panthi, S.M. Allard, A.R. Sapkota, A. Sapkota, Impact of high precipitation and temperature events on the distribution of emerging contaminants in surface water in the mid-atlantic, United States, Sci. Total Environ. 755 (2021) 142552.
[4] A. Ruhi, V. Acuna, D. Barcelo, B. Huerta, J.R. Mor, S. Rodriguez-Mozaz, S. Sabater, Bioaccumulation and trophic magnification of pharmaceuticals and endocrine disruptors in a mediterranean river food web, Sci. Total Environ. 540 (2016) 250–259.
[5] A. Zenker, M.R. Cicero, F. Prestinaci, P. Bottoni, M. Carere, Bioaccumulation and biomagnification potential of pharmaceuticals with a focus to the aquatic environment, J. Environ. Manag. 133 (2014) 378–387.
[6] M. Coccia, E. Bontempi, New trajectories of technologies for the removal of pollutants and emerging contaminants in the environment, Environ. Res. 229 (2023).
[7] J.F.J.R. Pesqueira, M.F.R. Pereira, A.M.T. Silva, Environmental impact assessment of advanced urban wastewater treatment technologies for the removal of priority substances and contaminants of emerging concern: a review, J. Clean. Prod. 261 (2020).
[8] B.S. Rathi, P.S. Kumar, P.L. Show, A review on effective removal of emerging contaminants from aquatic systems: current trends and scope for further research, J. Hazard Mater. 409 (2021) 124413.
[9] T. Suzuki, T. Hidaka, Y. Kumagai, M. Yamamoto, Environmental pollutants and the immune response, Nat. Immunol. 21 (12) (2020) 1486–1495.
[10] M. Kumar, S. Sridharan, A.D. Sawarkar, A. Shakeel, P. Anerao, G. Mannina, P. Sharma, A. Pandey, Current research trends on emerging contaminants pharmaceutical and personal care products (PPCPs): a comprehensive review, Sci. Total Environ. 859 (2023).
[11] L. Lyu, L. Zhang, Q. Wang, Y. Nie, C. Hu, Enhanced Fenton catalytic efficiency of gamma-Cu-Al_2O_3 by sigma-Cu^{2+}-ligand complexes from aromatic pollutant degradation, Environ. Sci. Technol. 49 (14) (2015) 8639–8647.
[12] S. Zhan, H. Zhang, X. Mi, Y. Zhao, C. Hu, L. Lyu, Efficient Fenton-like process for pollutant removal in electron-rich/poor reaction sites induced by surface oxygen vacancy over cobalt-zinc oxides, Environ. Sci. Technol. 54 (13) (2020) 8333–8343.
[13] P.R. Rout, T.C. Zhang, P. Bhunia, R.Y. Surampalli, Treatment technologies for emerging contaminants in wastewater treatment plants: a review, Sci. Total Environ. 753 (2021) 141990.
[14] S.F. Ahmed, M. Mofijur, S. Nuzhat, A.T. Chowdhury, N. Rafa, M.A. Uddin, A. Inayat, T.M.I. Mahlia, H.C. Ong, W.Y. Chia, P.L. Show, Recent developments in physical, biological, chemical, and hybrid treatment techniques for removing emerging contaminants from wastewater, J. Hazard Mater. 416 (2021).
[15] L. Rizzo, S. Malato, D. Antakyali, V.G. Beretsou, M.B. Đolić, W. Gernjak, E. Heath, I. Ivancev-Tumbas, P. Karaolia, A.R. Lado Ribeiro, G. Mascolo, C.S. McArdell, H. Schaar, A.M.T. Silva, D. Fatta-Kassinos, Consolidated vs new advanced treatment methods for the removal of contaminants of emerging concern from urban wastewater, Sci. Total Environ. 655 (2019) 986–1008.
[16] Z.F. Ma, H.L. Cao, F.C. Lv, Y. Yang, C. Chen, T.X. Yang, H.X. Zheng, D.S. Wu, Preparation of nZVI embedded modified mesoporous carbon for catalytic persulfate to degradation of reactive black 5, Front. Environ. Sci. Eng. 15 (2021).
[17] S.E.H. Mehdi, R. Amen, A. Ali, H. Anjum, A. Mahmood, M. Mubashir, A. Mukhtar, S. Ullah, A.G. Al-Sehemi, M. Ibrahim, M.S. Khan, M.A. Qyyum, P.L. Show, Sources, chemistry, bioremediation and social aspects of arsenic-contaminated waters: a review, Environ. Chem. Lett. 19 (5) (2021) 3859–3886.
[18] G.-F. Norra, J. Radjenovic, Removal of persistent organic contaminants from wastewater using a hybrid electrochemical-granular activated carbon (GAC) system, J. Hazard Mater. 415 (2021).
[19] L.H. Gao, Y.J. Cao, L.Z. Wang, S.L. Li, A review on sustainable reuse applications of Fenton sludge during wastewater treatment, Front. Environ. Sci. Eng. 16 (2022).
[20] Y. Wang, P. Zhang, L. Lyu, W. Liao, C. Hu, Efficient destruction of humic acid with a self-purification process in an Fe^0-Fe_yC_z/Fe_x-GZIF-8-rGO aqueous suspension, Chem. Eng. J. 446 (2022) 136625.
[21] T. Li, L. Zhang, Y. Gao, X. Xing, X. Zhang, F. Li, C. Hu, Detoxification and selective separation of Cr(VI) and As(III) in wastewater based on interfacial coupling in BiOBr with {110} facet under visible-light irradiation, Appl. Catal. B Environ. 307 (2022) 121192.
[22] F. Li, Z. Lu, T. Li, P. Zhang, C. Hu, Origin of the excellent activity and selectivity of a single-atom copper catalyst with unsaturated Cu-N_2 Sites via peroxydisulfate activation: Cu(III) as a dominant oxidizing species, Environ. Sci. Technol. (2022) 8765–8775.
[23] O.M. Rodriguez-Narvaez, J.M. Peralta-Hernandez, A. Goonetilleke, E.R. Bandala, Treatment technologies for emerging contaminants in water: a review, Chem. Eng. J. 323 (2017) 361–380.
[24] S. Xue, S.B. Sun, W.H. Qing, T.B. Huang, W. Liu, C.Q. Liu, H. Yao, W. Zhang, Experimental and computational assessment of 1,4-Dioxane degradation in a photo-Fenton reactive ceramic membrane filtration process, Front. Environ. Sci. Eng. 15 (2021).
[25] F. Liu, Y. Liu, Q. Yao, Y. Wang, X. Fang, C. Shen, F. Li, M. Huang, Z. Wang, W. Sand, J. Xie, Supported atomically-precise gold nanoclusters for enhanced flow-through electro-Fenton, Environ. Sci. Technol. 54 (9) (2020) 5913–5921.
[26] F. Li, T. Li, L. Zhang, Y. Jin, C. Hu, Enhancing photocatalytic performance by direct photo-excited electron transfer from organic pollutants to low-polymerized graphitic carbon nitride with more C-NH/NH_2 exposure, Appl. Catal. B Environ. 296 (2021) 120316.
[27] Y. Gu, T. Gao, F. Zhang, C. Lu, W. Cao, Z. Fu, C. Hu, L. Lyu, Surface sulfur vacancies enhanced electron transfer over Co-ZnS quantum dots for efficient degradation of plasticizer micropollutants by peroxymonosulfate activation, Chin. Chem. Lett. 33 (8) (2021) 3829–3834.
[28] P. Villegas-Guzman, J. Silva-Agredo, A.L. Giraldo-Aguirre, O. Florez-Acosta, C. Petrier, R.A. Torres-Palma, Enhancement and inhibition effects of water matrices during the sonochemical degradation of the antibiotic dicloxacillin, Ultrason. Sonochem. 22 (2015) 211–219.
[29] Y. Wang, P. Zhang, T. Li, L. Lyu, Y. Gao, C. Hu, Enhanced Fenton-like efficiency by the synergistic effect of oxygen vacancies and organics adsorption on Fe_xO_y-d-g-C_3N_4 with FeN complexation, J. Hazard Mater. 408 (2021) 124818.
[30] A. Lagutschenkov, R.K. Sinha, P. Maitre, O. Dopfer, Structure and infrared spectrum of the Ag^+-Phenol ionic complex, J. Phys. Chem. A 114 (42) (2010) 11053–11059.
[31] M.A. Gebbie, W. Wei, A.M. Schrader, T.R. Cristiani, H.A. Dobbs, M. Idso, B.F. Chmelka, J.H. Waite, J.N. Israelachvili, Tuning underwater adhesion with cation-pi interactions, Nat. Chem. 9 (5) (2017) 473–479.
[32] L. Lyu, G. Yu, L. Zhang, C. Hu, Y. Sun, 4-Phenoxyphenol-functionalized reduced graphene oxide nanosheets: a metal-free Fenton-like catalyst for pollutant destruction, Environ. Sci. Technol. 52 (2) (2018) 747–756.
[33] L. Lyu, D. Yan, G. Yu, W. Cao, C. Hu, Efficient destruction of pollutants in water by a dual-reaction-center fenton-like process over carbon nitride compounds-complexed Cu(II)-$CuAlO_2$, Environ. Sci. Technol. 52 (7) (2018) 4294–4304.
[34] C. Lu, K. Deng, C. Hu, L. Lyu, Dual-reaction-center catalytic process continues Fenton's story, Front. Environ. Sci. Eng. 14 (5) (2020).
[35] K. Deng, T. Gao, Q. Fang, F. Wu, C. Lu, F. Zhang, W. Cao, M. Han, C. Hu, L. Lyu, Vanadium tetrasulfide cross-linking graphene-like carbon driving a sustainable electron supply chain from pollutants through the activation of dissolved oxygen and hydrogen peroxide, Environ. Sci.: Nano 8 (1) (2021) 86–96.
[36] C. Li, X. Cai, Q. Fang, Y. Luo, P. Zhang, C. Lu, M. Han, C. Hu, L. Lyu, Peroxymonosulfate as inducer driving interfacial electron donation of pollutants over oxygen-rich carbon-nitrogen graphene-like nanosheets for water treatment, J. Colloid Interface Sci. 622 (2022) 272–283.
[37] K. Deng, Y. Gu, T. Gao, Z. Liao, Y. Feng, S. Zhou, Q. Fang, C. Hu, L. Lyu, Carbonized MOF-coated zero-valent Cu driving an efficient dual-reaction-

center Fenton-like water treatment process through utilizing pollutants and natural dissolved oxygen, ACS ES&T Water 2 (1) (2021) 174–183.
[38] C. Lu, Q. Fang, C. Hu, L. Lyu, Sustainable micro-activation of dissolved oxygen driving pollutant conversion on Mo-enhanced zinc sulfide surface in natural conditions, Fundam. Res. 3(3) (2023) 422–429.
[39] W. Cao, C. Hu, L. Lyu, Efficient decomposition of organic pollutants over nZVI/FeO_x/FeN_y-anchored NC layers via a novel dual-reaction-centers-based wet air oxidation process under natural conditions, ACS ES&T Eng. 1 (9) (2021) 1333–1341.
[40] X. Zhao, X. Ma, B. Chen, Y. Shang, M. Song, Challenges toward carbon neutrality in China: strategies and countermeasures, Resour. Conserv. Recycl. 176 (2022).
[41] J. Yan, Y. Huang, Y. Yan, X. Zhao, P. Liu, The composition design of MOF-derived Co-Fe bimetallic autocatalysis carbon nanotubes with controllable electromagnetic properties, Compos Part A-appl S 139 (2020) 106107.
[42] X. Luo, H. Ma, H. Ren, X. Zou, Y. Wang, X. Li, Z. Shen, Y. Wang, L. Cui, Controllable synthesis of nitrogen-doped carbon containing Co and Co_3Fe_7 nanoparticles as effective catalysts for electrochemical oxygen conversion, J. Colloid Interface Sci. 590 (2021) 622–631.
[43] T. Palaniselvam, V. Kashyap, S.N. Bhange, J.-B. Baek, S. Kurungot, Nanoporous graphene enriched with Fe/Co-N active sites as a promising oxygen reduction electrocatalyst for anion exchange membrane fuel cells, Adv. Funct. Mater. 26 (13) (2016) 2150–2162.
[44] Z.-H. Sheng, L. Shao, J.-J. Chen, W.-J. Bao, F.-B. Wang, X.-H. Xia, Catalyst-free synthesis of nitrogen-doped graphene via thermal annealing graphite oxide with melamine and its excellent electrocatalysis, ACS Nano 5 (6) (2011) 4350–4358.
[45] H. Ji, M. Wang, S. Liu, H. Sun, J. Liu, T. Qian, C. Yan, Pyridinic and graphitic nitrogen-enriched carbon paper as a highly active bifunctional catalyst for Zn-air batteries, Electrochim. Acta 334 (2020) 135562.
[46] K. Sakaushi, A. Lyalin, S. Tominaka, T. Taketsugu, K. Uosaki, Two-dimensional corrugated porous carbon-, nitrogen-framework/metal heterojunction for efficient multielectron transfer processes with controlled kinetics, ACS Nano 11 (2) (2017) 1770–1779.
[47] X. Gu, Z. Chen, Y. Li, J. Wu, X. Wang, H. Huang, Y. Liu, B. Dong, M. Shao, Z. Kang, Polyaniline/Carbon dots composite as a highly efficient metal-free dual-functional photoassisted electrocatalyst for overall water splitting, ACS Appl. Mater. Interfaces 13 (21) (2021) 24814–24823.
[48] W. Cheng, P. Yuan, Z. Lv, Y. Guo, Y. Qiao, X. Xue, X. Liu, W. Bai, K. Wang, Q. Xu, J. Zhang, Boosting defective carbon by anchoring well-defined atomically dispersed metal-N_4 sites for ORR, OER, and Zn-air batteries, Appl. Catal. B Environ. 260 (2020) 118198.
[49] L. Lyu, W. Cao, G. Yu, D. Yan, K. Deng, C. Lu, C. Hu, Enhanced polarization of electron-poor/rich micro-centers over nZVCu-Cu(II)-rGO for pollutant removal with H_2O_2, J. Hazard Mater. 383 (2020) 121182.
[50] Y. Wang, H. Wang, J. Ye, L. Shi, X. Feng, Magnetic CoFe alloy@C nanocomposites derived from ZnCo-MOF for electromagnetic wave absorption, Chem. Eng. J. 383 (2020) 123096.
[51] Y. Gao, Y. Zhu, L. Lyu, Q. Zeng, X. Xing, C. Hu, Electronic structure modulation of graphitic carbon nitride by oxygen doping for enhanced catalytic degradation of organic pollutants through peroxymonosulfate Activation, Environ. Sci. Technol. 52 (24) (2018) 14371–14380.
[52] L. Lyu, L. Zhang, G. He, H. He, C. Hu, Selective H_2O_2 conversion to hydroxyl radicals in the electron-rich area of hydroxylated C-g-C_3N_4/CuCo–Al_2O_3, J. Mater. Chem. A 5 (15) (2017) 7153–7164.
[53] Y. Xu, M. Chen, T. Wang, B. Liu, F. Jiang, X. Liu, Probing cobalt localization on HZSM-5 for efficient methane dehydroaromatization catalysts, J. Catal. 387 (2020) 102–118.
[54] L. Wang, M. Chen, X. Yu, Z. Zhao, X. Fan, Y. Wei, J. Liu, Preparation, characterization and catalytic performance of ordered macroporous-mesoporous SiO_2-supported $MnMO_x$ catalysts for soot combustion, Catal. Today 364 (2021) 21–34.
[55] E.S. Lokteva, V.V. Shishova, N.N. Tolkachev, A.N. Kharlanov, K.I. Maslakov, A.O. Kamaev, I.Y. Kaplin, I.N. Savina, E.V. Golubina, Hydrodechlorination of 4-chlorophenol on Pd-Fe catalysts on mesoporous ZrO_2SiO_2 support, Molecules 26 (1) (2020) 141.
[56] Q. Zhao, S. Huang, X. Han, J. Chen, J. Wang, A. Rykov, Y. Wang, M. Wang, J. Lv, X. Ma, Highly active and controllable MOF-derived carbon nanosheets supported iron catalysts for Fischer-Tropsch synthesis, Carbon 173 (2021) 364–375.
[57] W. Cao, Z. Wang, P. Zhang, Y. Sun, Z. Xie, C. Hu, S. Wang, G. Huang, L. Lyu, Water self-purification with zero external consumption by livestock manure resource utilization, Environ. Sci. Technol. 57 (7) (2023) 2837–2845.
[58] L. Lyu, C. Lu, Y. Sun, W. Cao, T. Gao, C. Hu, Low consumption Fenton-like water purification through pollutants as electron donors substituting H_2O_2 consumption via twofold cation-π over MoS_2 cross-linking g-C_3N_4 hybrid, Appl. Catal. B Environ. 320 (2023) 121871.
[59] Y. Shi, Z. Xie, C. Hu, L. Lyu, Resourcelized conversion of livestock manure to porous cage microsphere for eliminating emerging contaminants under peroxymonosulfate trigger, iScience 26 (3) (2023) 106139.
[60] J. Wang, S. Wang, Reactive species in advanced oxidation processes: formation, identification and reaction mechanism, Chem. Eng. J. 401 (2020) 126158.